Eur. Phys. J. E (2012) **35**: 32
DOI 10.1140/epje/i2012-12032-y

THE EUROPEAN PHYSICAL JOURNAL E

Regular Article

Biaxial surface order dynamics in calamitic nematics

G. Lombardo[1], A. Amoddeo[2], R. Hamdi[3], H. Ayeb[3,4], and R. Barberi[1,3,a]

[1] CNR-IPCF UOS di Cosenza, c/o University of Calabria, 87036 Rende, Italy
[2] Mechanics and Materials Department, University "Mediterranea" of Reggio Calabria, 89122 Reggio Calabria, Italy
[3] Physics Department, University of Calabria, 87036 Rende, Italy
[4] Département de Physique, Laboratoire de Physique de la Matière Molle, Faculté des Sciences de Tunis, Université de Tunis El Manar, 2092 Tunis, Tunisia

Received 19 January 2012 and Received in final form 19 March 2012
Published online: 17 May 2012

Abstract. Thermotropic nematic materials relax strong distortions by lowering the nematic order: the uniaxial symmetry is broken and is locally replaced by biaxial domains. We investigated the dynamics of the nematic order near a boundary surface of an asymmetric π-cell submitted to an external electric field, close to the electric order reconstruction threshold. An unexpected phenomenon is observed close, but below the threshold: the biaxial order spreads on the surface inducing a consequent bulk topological behaviour equivalent to the splay-bend fast transition allowed by order reconstruction at higher voltage.

1 Introduction

A calamitic mesogen molecule is the most common building block of a thermotropic Nematic Liquid Crystal (NLC) and it consists essentially of a flat rigid core with flexible side chains. The core is responsible of mesophase anisotropy, whereas terminal chains contribute to stabilize the molecular order. Physicists usually represent these complex molecules as simple rods with cylindrical symmetry, taking into account the average shape also given by the fast thermal rotational motion around their main axis. Therefore, most of NLCs phenomena are described by the dimensionless unit vector $\mathbf{n}$, the director, which indicates the average orientation of rod-like calamitic building blocks, and by the uniaxial scalar order parameter S [1]. This approach is widely used because it can successfully describe most of electro-optical behaviours of nematics. Nevertheless, rich and intriguing physical phenomena in highly frustrated NLC systems, such as topological defects [2–4], self-organized colloidal dispersions [5–7], emulsions [8], confinement in porous materials [9] or in micrometric topographic patterns [10] cannot be fully explained by the classical model, and a tensor order parameter $\mathbf{Q}$, which couples $\mathbf{n}$ and S, needs to be defined [11]. The tensor description predicts two different ordered phases for NLC: uniaxial, with a cylindrical symmetry around the director, and biaxial, where the symmetry presents two distinct axes. Several mechanisms can originate biaxial order in usual calamitic NLC [3,12–14] with bulk- or surface-related phenomena [15–18]. Examples are the π-cell, where a strong enough electric field induces a thin two-dimensional biaxial wall in the bulk [19–22], or the structural transition, with the appearance of surface biaxial order, that has been observed when a nematic topological defect is nano-confined between two competing alignment surfaces [23]. The electrically induced nematic order reconstruction has also been investigated for an asymmetric π-cell with strong anchoring conditions [24], and the electrically induced biaxial wall occurred close to the surface plate with smaller pretilt, with effects similar to anchoring breaking, [25] demanding further investigations [26].

2 Numerical model

A π-cell has a sandwich geometry, with a thin film of nematic confined between two flat glass plates. The alignment on both surfaces induces a uniform pretilt angle and the two plates are oriented to admit two topological different equilibrium nematic textures: a slight splay state, without torsion, and a bend texture, topologically equivalent to a π-twisted texture[1]. In this work, we study how the nematic distortion, induced by a strong electric field, evolves inside an asymmetric π-cell and it is lowered by the appearance of biaxial order close to a boundary surface.

The NLC orientation and order are described by a second rank tensor order parameter $\mathbf{Q}$ and its dynamics is

[a] e-mail: riccardo.barberi@fis.unical.it

[1] Higher-order twisted states are also possible, but the analysis is here restricted to the two textures with lowest elastic energy.

governed by a balance between the dissipation and the free-energy variation [27]. If the NLC is considered as a pure dielectric material and ions effects are neglected, the free energy F of the system includes the distortion elastic energy F_d, the bulk free energy F_t of the nematic phase and the electrostatic energy F_e due to the external electric field. The interaction with the bounding surfaces is imposed by Dirichlet conditions, as this work is made in the limit of infinite anchoring energy. To solve the governing dynamical equations system, we minimize F using the finite-element method [28]: the spatial domain is discretized with one-dimensional elements of size 1 nm and we use a time step of 1 μs to monitor the dynamical evolution of the nematic distortion. Starting from the time solution of $\mathbf{Q}$, we evaluate the director orientation, that is the orientation of the eigenvector associated to the maximum eigenvalue of $\mathbf{Q}$, the induced biaxial order $\beta = \sqrt{1 - \frac{6[\mathrm{tr}(\mathbf{Q}^3)]^2}{[\mathrm{tr}(\mathbf{Q}^2)]^3}}$, the scalar order parameter S, proportional to the maximum eigenvalue of $\mathbf{Q}$. β is a convenient parameter for monitoring the spatial inhomogeneities of $\mathbf{Q}$ and hence the order dynamics: β varies between 0 (uniaxial texture) and 1 (maximum biaxiality). Moreover we calculated the electric current density [19], which flows across the cell, by using $J = \frac{V}{d}\frac{\partial}{\partial t}\left(\frac{1}{\mathrm{eff}^{-1}}\right)$, where V is the amplitude of the applied voltage, which generates an electric field perpendicular to the boundary plates, d is the cell thickness and eff^{-1} is the effective electrical permittivity average expressed as $\mathrm{eff}^{-1} = \frac{1}{d}\int_0^d \frac{1}{\varepsilon_0(\Delta\varepsilon\cdot Q_{zz}+\varepsilon^{\mathrm{iso}})}\mathrm{d}z$, where ε_0 is the vacuum permittivity, $\Delta\varepsilon = \frac{\varepsilon_\parallel - \varepsilon_\perp}{S}$ is the scaled dielectric anisotropy, and $\varepsilon^{\mathrm{iso}}$ is an average permittivity expressed as $\frac{\varepsilon_\parallel + 2\varepsilon_\perp}{3}$. $\varepsilon_\parallel$ and $\varepsilon_\perp$ are the parallel and perpendicular dielectric constants, respectively.

The numerical simulations were carried out with the physical parameters of 5CB (4-n-pentyl-4-cyano biphenyl) at $T = 32\,^\circ$C [29], obtaining an electric threshold for the order reconstruction phenomenon of $E_{\mathrm{th}} = 16\,\mathrm{V}/\mu\mathrm{m}$. The pretilt angles on the two boundary surfaces of the asymmetric π-cell of thickness 1 μm were 19° and 1° for the upper and the lower plate, respectively. The analysis has been made for two different amplitudes of the vertical electric field: a) $17\,\mathrm{V}/\mu\mathrm{m}$, above E_{th}, and b) $14\,\mathrm{V}/\mu\mathrm{m}$, below E_{th}. At $t = 0$ s, the nematic director presents a starting asymmetric splay texture with the nematic planar plane close to the lower surface with smaller pretilt. The application of the electric field for $t > 0$ s changes the initial configuration and the induced nematic distortion relaxes in two different ways, depending on the amplitude of the electric field, see fig. 1. As the anchoring energy on both surfaces is strong, surface molecules hold their positions, whereas the nematic director in the bulk tends to be aligned along the electric field ($\Delta\varepsilon_{5\mathrm{CB}} > 0$).

2.1 Numerical results

Figure 1(a) and fig. 2(a) show the theoretical evolution of the nematic director and of the biaxiality, respectively, when the field is above E_{th}. For $t < 30\,\mu$s, nematic molecules are reoriented along the vertical electric field and, for symmetry, the nematic distortion tends to be concentrated near the lower surface forming a π-wall. Similarly the biaxial order propagates from the bulk and it is concentrated on the thin π-biaxial wall. For $20\,\mu\mathrm{s} < t < 30\,\mu$s, the wall has a dimension comparable with the electric coherence length ξ_E [1], which compares with the biaxial coherence length ξ_b [19], in the order of 10 nm, and the nematic order in the wall is mainly biaxial with $\beta = 1$. $\xi_b = \sqrt{\frac{K}{b\,S^3}}$, where b is the phenomenological coefficient of the third power term of the bulk free-energy potential and K is an elastic constant [13,30]. Most of the nematic strain is concentrated in the biaxial wall. At time $t \approx 30\,\mu$s the planar wall suddenly disappears, due to the order reconstruction dynamics, and a π-bend texture replaces the initial splay texture [19]. This fast transition lets the topological barrier between the splay texture and the bend one to be overcome. For $t > 30\,\mu$s, the simulated domain presents only a residual thin biaxial region close to the low pretilt boundary surface.

If the applied electric field is not strong enough to induce the order reconstruction, the planar wall is pushed towards the adjacent surface with smaller pretilt by the re-orientation of bulk nematic molecules, see fig. 1(b). The nematic texture is practically uniaxial for $0\,\mu\mathrm{s} < t < 10\,\mu$s; for $t > 10\,\mu$s the bulk biaxiality starts to develop, and then it propagates inside the cell: S becomes strongly inhomogeneous near the lower surface where β is growing, see fig. 2(b). The nematic distortion concentrates in the regions of lower S, where the elastic constants, which are proportional to S^2, present lower values: the nematic distortion relaxes in a thin surface region with a thickness comparable with ξ_b [3,18,23]. For $t > 40\,\mu$s, the nematic distortion is completely distributed on the lower surface: the appearance of the surface biaxial layer mediates the competition between the bulk reorientation due to the high electric field and the local order of the surface that cannot change due to strong anchoring conditions. The final nematic texture in the bulk looks like a π-bend texture but it has been obtained without order reconstruction or anchoring breaking.

The order dynamics is slower below E_{th} than above E_{th}, but in both cases one observes that the initial untwisted splay texture is replaced by a π-bend state in the bulk of the π-cell. Above E_{th}, the order reconstruction dynamics cancels the biaxial order and let to connect the two topological distinct splay and bend textures by a fast transition; on the contrary, below E_{th}, the biaxial order spreads on the lower boundary layer and the bulk splay textures is replaced continuously by an equivalent π-bend texture. Such behaviour is reminiscent of the surface defect spreading in hybrid homeotropic-planar cells under nanoconfinement [23] or in the presence of strong electric field [28] and provides a bulk texture transition equivalent to the anchoring breaking phenomenon [24,25], but the strain now does not disappear and it remains concentrated on the boundary surface.

It has been demonstrated experimentally as well as theoretically that the electric response of a symmetric

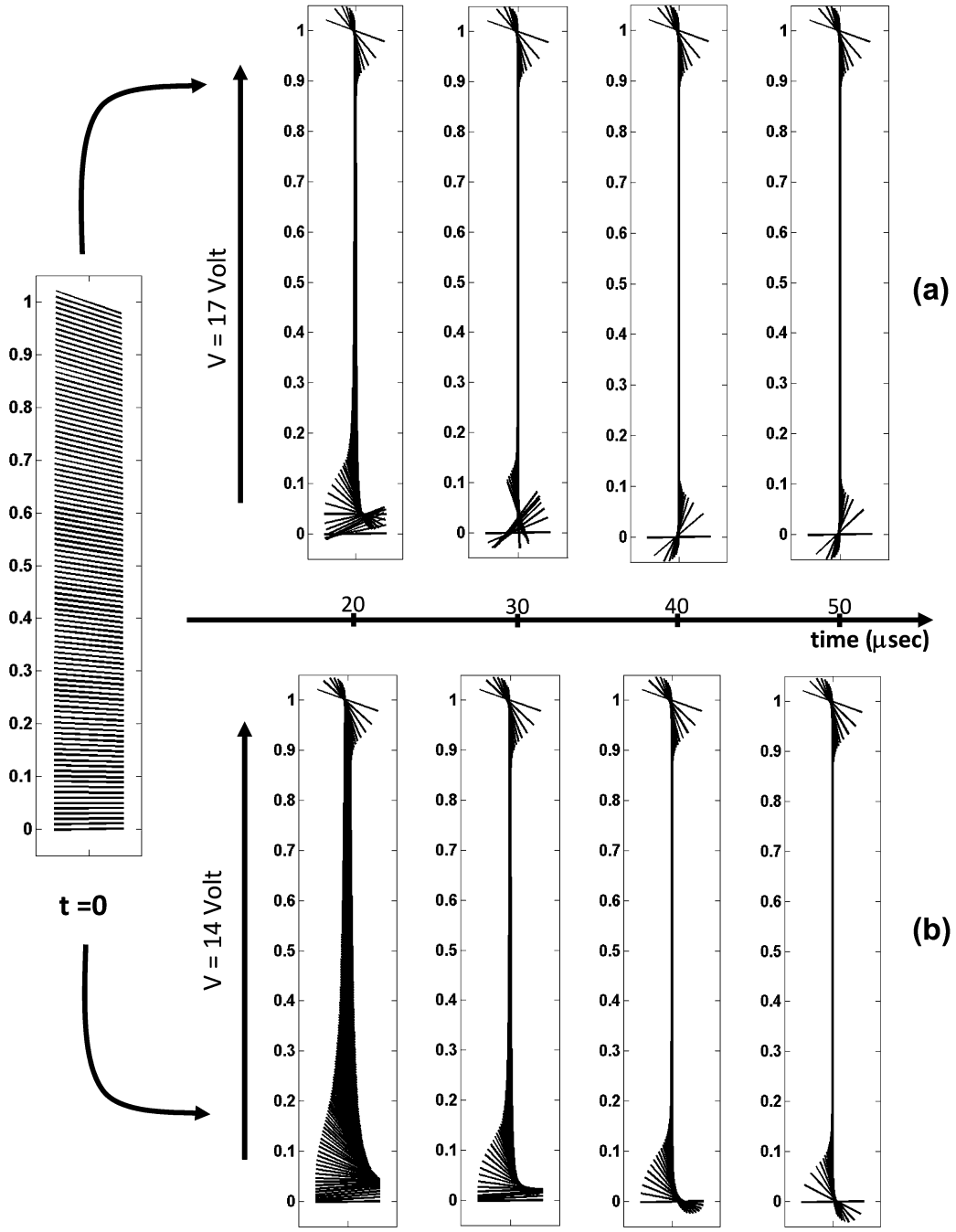

Fig. 1. Director evolution within an asymmetric π-cell of thickness 1 μm for two different electric field amplitudes: 17 V/μm (a), above $E_{\rm th}$, and 14 V/μm (b), below $E_{\rm th}$. In (a) the bulk order reconstruction transition allows to overcome the topological barrier between the splay and bend textures, the π-wall disappears by order reconstruction and the main nematic strain is relaxed; (b) the bulk splay-bend transition occurs by a slower movement of the biaxial π-wall spreading on the boundary surface, saving the original surface nematic orientation and without relaxing the strain.

π-cell is very sensitive to the nematic order dynamics and the analysis of the current signal provides relevant data about the induced biaxiality [19–21,31,32]. The electric current features allow to distinguishing the dynamical order behaviours above $E_{\rm th}$ and below $E_{\rm th}$. Figure 3(a) shows the calculated electric current flowing across the asymmetric π-cell for the two different applied electric amplitudes E: 14 V/μm and 17 V/μm.

Nematics are insulating media and their electrical conduction is principally due to ions, by molecular dissociation or by external contamination. Nevertheless ions concentration in pure 5CB is found to be quite low [33,34] and

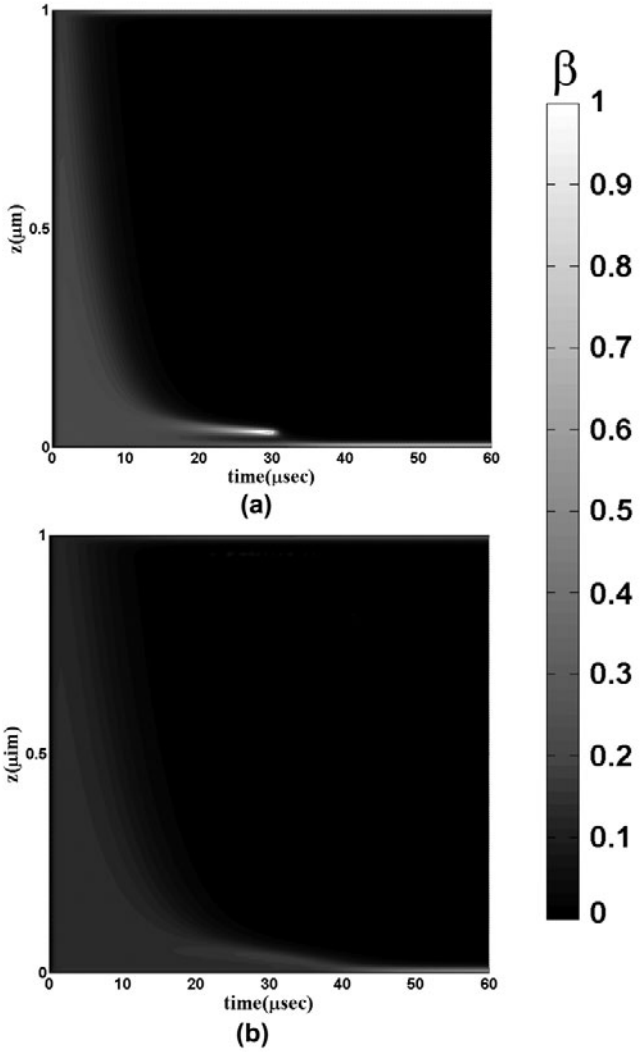

Fig. 2. Biaxial order evolution within an asymmetric π-cell of thickness $1\,\mu$m for two different electric field amplitudes: $17\,\mathrm{V}/\mu$m (a), above E_{th}, and $14\,\mathrm{V}/\mu$m (b), below E_{th}. The biaxiality β is linearly mapped in a grey level scale between 0 (black) and 1 (white). The vertical axis represents the cell thickness; the time is represented along the horizontal axis.

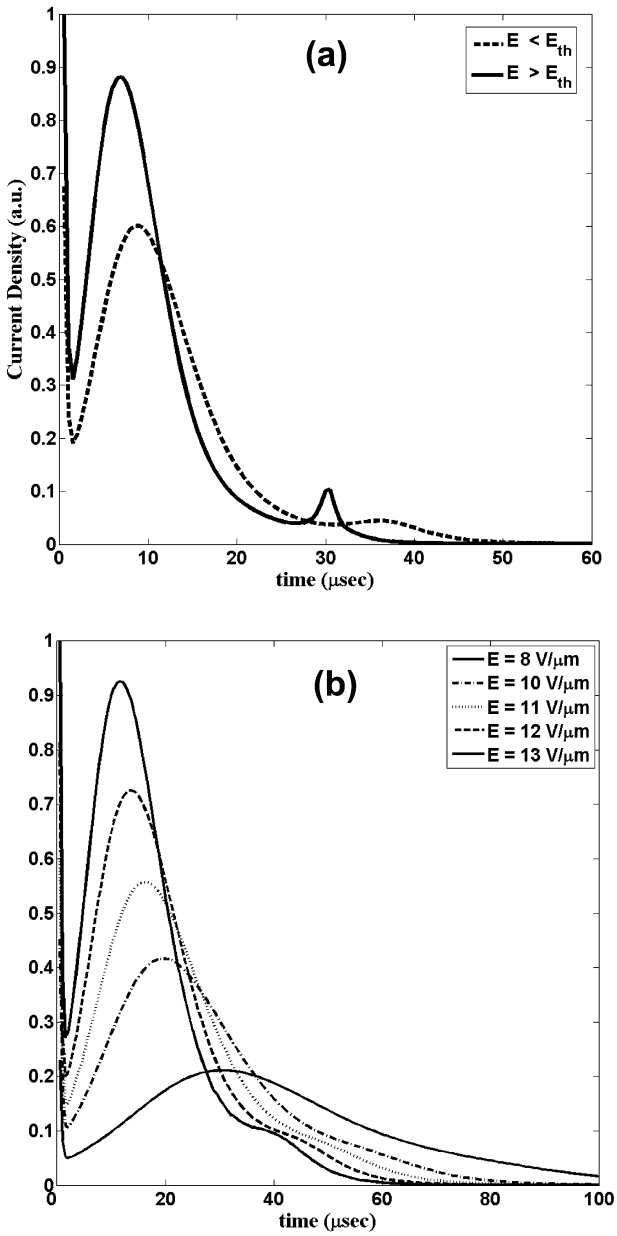

Fig. 3. (a) Numerical evaluation of the electric current flowing across the asymmetric π-cell *vs.* time (a) for two electric field amplitudes: $14\,\mathrm{V}/\mu$m, below E_{th} (dashed line) and $17\,\mathrm{V}/\mu$m, above E_{th} (continuous line); (b) for five electric field amplitudes below E_{th}.

hence 5CB can be considered as a pure dielectric material. Moreover, ionic and order reconstruction contributions to the electric current flowing across the π-cell are always distinguishable by means of a suitable time-resolved analysis [20].

In fig. 3(a), two peaks are well defined when the applied electric field is above E_{th}: the fastest and largest one is due to dielectric realignment of nematic molecules along the electric field for $0 < t < 20\,\mu$s, while the second one has a time duration of approximately $5\,\mu$s. The appearance of this second pulse is related to the breaking of the biaxial wall at $t = 30\,\mu$s, due to order reconstruction [19–21,31, 32], see also fig. 2(a). On the other hand, below E_{th}, only one well-defined peak, followed by a smooth longer current structure is present: the well-defined fast and large peak is due again to dielectric realignment of nematic molecules along the electric field for $0 < t < 30\,\mu$s, while the following larger signal, whose maximum amplitude occurs at about $t = 38\,\mu$s, is due to the slow movement of the planar wall towards the lower surface layer, see also fig. 2(b). This second current structure tends to become larger and slower for lower applied electric field becoming practically disappearing far enough from E_{th}, see fig. 3(b).

3 Experimental observations

For a better understanding of these behaviours, we prepared a sandwich asymmetric π-cell of about $2\,\mu$m thick-

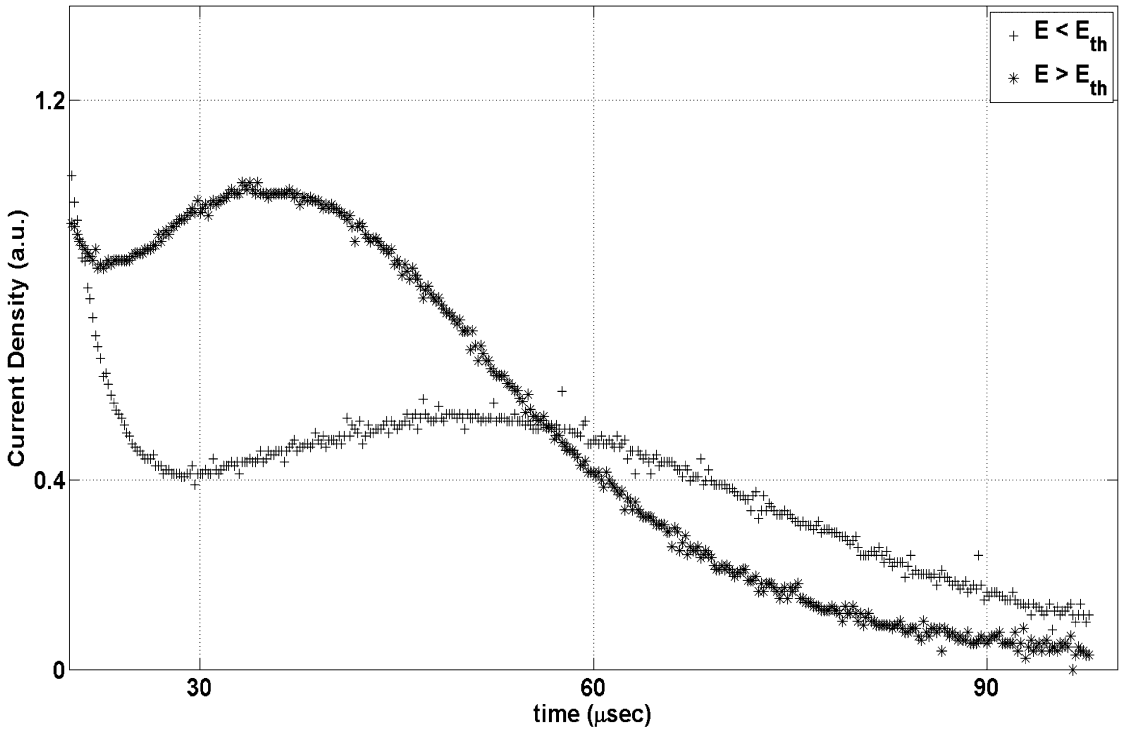

Fig. 4. Experimental measurements of the electric current flowing across an asymmetric π-cell *vs.* time for two values of the electric field: $15\,\mathrm{V}/\mu\mathrm{m}$ (grey data points, crosses) and $17\,\mathrm{V}/\mu\mathrm{m}$ (black data points, asterisks).

ness, made with two parallel transparent indium tin oxide (ITO)-coated glass plates filled with 5CB. Suitable electrodes were obtained by photolithographic treatment of the ITO film on the two plates: the etching stripes were 1 mm wide and their crossed superposition gave one pixel of about $1\,\mathrm{mm}^2$ area. The cell had a boundary surface coated by a mixture of 20% weight of polyimide in pyrrolidinone. This mixture was deposed by spin coating, oven dried and then unidirectional rubbed to have a strong anchoring with a pretilt of about 8°. The other plate was treated in a similar way with a mixture of 2% weight of polyimide in pyrrolidinone for strong anchoring with a smaller pretilt of about 2°. The cell was submitted to a square electric pulse of duration $\tau = 1\,\mathrm{ms}$ and amplitude E and the measured electric order reconstruction threshold was $E_{\mathrm{th}} = 16\,\mathrm{V}/\mu\mathrm{m}$ [24]. Figure 4 shows the electric current flowing in the cell after the dielectric reorientation peak in two cases: black data points correspond to $E = 17\,\mathrm{V}/\mu\mathrm{m} > E_{\mathrm{th}}$, whereas grey data points correspond to $E = 15\,\mathrm{V}/\mu\mathrm{m} < E_{\mathrm{th}}$. Figure 4 shows only the electric behaviour after the large dielectric peak to highlight the different behaviours above and below the order reconstruction threshold. Above E_{th}, the electric current presents a quite well-defined peak of about $10\,\mu\mathrm{s}$ duration, while, below E_{th}, the current response is about three times longer, confirming the different behaviour of induced order reconstruction above E_{th} and the spreading of the biaxial wall on the boundary plate with smaller pretilt below E_{th} as predicted by the calculated results shown in fig. 3. In this comparison, one should take also into account that the electric peak response corresponding to order reconstruction should be even faster than what reported in fig. 4, but any inhomogeneity in the cell, usual for surface phenomena, can result in a defect-mediated order reconstruction rather than in a uniform transition, spreading the electric response [22]. For lower applied electric field this electric current structure becomes larger and larger with a monotone amplitude decrease, becoming not well resolved from the main signal of the electric current itself.

4 Conclusions

In conclusion, both theoretical analysis and experiments have shown that, above E_{th}, the energy of the biaxial wall is released in a short time, building a well-defined dielectric peak in the electric current, corresponding to the well-known order reconstruction phenomenon, whereas, below E_{th}, the energy is released more slowly by the motion of the biaxial wall spreading on the low pretilt surface plate, with a wider electric signal. This second phenomenon presents an unexpected and not obvious behaviour and it has been also randomly observed in experiments carried out by means of a two-photons fluorescence microscope [35]. This effect is reminiscent of the surface defect spreading in hybrid homeotropic-planar cells in the presence of a strong electric field [28] or under nanoconfinement [23] and of anchoring breaking [25], demonstrating that biaxiality plays an important role at the nematic interface with a substrate, where the symmetry of NLC bulk is spontaneously broken. These results enlarge our understanding of the role of the nematic order

in highly frustrated systems and improve the knowledge of the surface-nematic interaction in order to control biaxial nematic properties and to design novel optical devices with, for instance, intrinsic bistability, granted by the energy barrier between topologically distinct states.

This research has been partially supported by the Italian Research Project of High National Interest (PRIN 2008) n. 2008F3734A.

References

1. P.G. de Gennes, J. Prost, *The Physics Liquid Crystals* (Clarendon Press, Oxford, 1993).
2. M. Kleman, O.D. Lavrentovich, Philos. Mag. **86**, 4117 (2006) DOI: 10.1080/14786430600593016.
3. N. Schopohl, T.J. Sluckin, Phys. Rev. Lett. **59**, 2582 (1987) DOI: 10.1103/PhysRevLett.59.2582.
4. M. Buscaglia, G. Lombardo, L. Cavalli, R. Barberi, T. Bellini, Soft Matter **6**, 5434 (2010) DOI: 10.1039/c0sm00578a.
5. I. Musevic, M. Skarabot, U. Tkalec, M. Ravnik, S. Zumer, Science **313**, 954 (2006) DOI: 10.1126/science.1129660.
6. I.I. Smalyukh, O.D. Lavrentovich, A.N. Kuzmin, A.V. Kachynski, P.N. Prasad, Phys. Rev. Lett. **95**, 157801 (2005) DOI: 10.1103/PhysRevLett.95.157801.
7. J.C. Loudet, P. Hanusse, P. Poulin, Science **306**, 1525 (2004) DOI: 10.1126/science.1102864.
8. E. Tjipto, K.D. Cadwell, J.F. Quinn, A.P.R. Johnston, N.L. Abbott, F. Caruso, Nano Lett. **6**, 2243 (2006) DOI: 10.1021/nl061604p.
9. F. Aliev, S. Basu, J. Non-Cryst. Solids **352**, 4983 (2006) DOI: 10.1016/j.jnoncrysol.2006.01.130.
10. Y.Yi, G. Lombardo, N. Ashby, R. Barberi, J.E. Maclennan, N.A. Clark, Phys. Rev. E **79**, 041701 (2009) DOI: 10.1103/PhysRevE.79.041701.
11. P.G. de Gennes, Phys. Lett. A **30**, 454 (1969).
12. M.J. Freiser, Phys. Rev. Lett. **24**, 1041 (1970) DOI: 10.1103/PhysRevLett.24.1041.
13. F. Ciuchi, H. Ayeb, G. Lombardo, R. Barberi, G. Durand, Appl. Phys. Lett. **91**, 244104 (2007) DOI: 10.1063/1.2824830.
14. H. Ayeb, F. Ciuchi, G. Lombardo, R. Barberi, Mol. Cryst. Liq. Cryst. **481**, 73 (2008) DOI: 10.1080/15421400701834096.
15. T. Qian, P. Sheng, Liq. Cryst. **26**, 229 (1999).
16. P. Martinot-Lagarde, H. Dreyfus-Lambez, I. Dozov, Phys. Rev. E **67**, 051710 (2003) DOI: 10.1103/PhysRevE.67.051710.
17. P. Biscari, G. Napoli, S. Turzi, Phys. Rev. E **74**, 031708 (2006) DOI: 10.1103/PhysRevE.74.031708.
18. M. Ambrozic, S. Kralj, E.G. Virga, Phys. Rev. E **75**, 031708 (2007) DOI: 10.1103/PhysRevE.75.031708.
19. R. Barberi, F. Ciuchi, G. Durand, M. Iovane, D. Sikharulidze, A. Sonnet, E. Virga, Eur. Phys. J. E **13**, 61 (2004) DOI: 10.1140/epje/e2004-00040-5.
20. R. Barberi, F. Ciuchi, G. Lombardo, R. Bartolino, G.E. Durand, Phys. Rev. Lett. **93**, 137801 (2004) DOI: 10.1103/PhysRevLett.93.137801.
21. R. Barberi, F. Ciuchi, H. Ayeb, G. Lombardo, R. Bartolino, G. Durand, Phys. Rev. Lett. **96**, 019802 (2006) DOI: 10.1103/PhysRevLett.96.019802.
22. G. Lombardo, H. Ayeb, F. Ciuchi, M.P. De Santo, R. Barberi, R. Bartolino, E.G. Virga, G. Durand, Phys. Rev. E **77**, 020702(R) (2008) DOI: 10.1103/PhysRevE.77.020702.
23. G. Carbone, G. Lombardo, R. Barberi, I. Musevic, U. Tkalec, Phys. Rev. Lett. **103**, 167801 (2009) DOI: 10.1103/PhysRevLett.103.167801.
24. H. Ayeb, G. Lombardo, F. Ciuchi, R. Hamdi, A. Gharbi, G. Durand, R. Barberi, Appl. Phys. Lett. **97**, 104104 (2010) DOI: 10.1063/1.3455885.
25. R. Barberi, G. Durand, Appl. Phys. Lett. **58**, 2907 (1991) DOI: 10.1063/1.104718.
26. C.H. Lee, E.P. Raynes, S.J. Elston, Appl. Phys. Lett. **97**, 153501 (2010) DOI: 10.1063/1.3502472.
27. A.M. Sonnet, E.G. Virga, Phys. Rev. E **64**, 031705 (2001) DOI: 10.1103/PhysRevE.64.031705.
28. G. Lombardo, H. Ayeb, R. Barberi, Phys. Rev. E **77**, 051708 (2008) DOI: 10.1103/PhysRevE.77.051708.
29. B. Ratna, R. Shashidhar, Mol. Cryst. Liq. Cryst. **42**, 1123 (1977).
30. S. Kralj, E.G. Virga, S. Zumer, Phys. Rev. E **60**, 1858 (1999) DOI: 10.1103/PhysRevE.60.1858.
31. A. Amoddeo, R. Barberi, G. Lombardo, Liq. Cryst. **38**, 93 (2011) DOI: 10.1080/02678292.2010.530298.
32. A. Amoddeo, R. Barberi, G. Lombardo, to be published in Phys. Rev. E.
33. P.P. Korneychuk, A.M. Gabovich, A.I. Voitenko, Yu.A. Reznikov, Ukr. J. Phys. **54**, 75 (2009).
34. R. Shah, N.L. Abbott, J. Phys. Chem. B **105**, 4936 (2001) DOI: 10.1021/jp004073g.
35. P.S. Salter, G. Carbone, E.J. Botcherby, T. Wilson, S.J. Elston, E.P. Raynes, Phys. Rev. Lett. **103**, 257803 (2009) DOI: 10.1103/PhysRevLett.103.257803.